Plasma Sci. Technol. **19** (2017) 095502 (10pp) https://doi.org/10.1088/2058-6272/aa6d6d

Methane conversion using a dielectric barrier discharge reactor at atmospheric pressure for hydrogen production

N KHADIR[1], **K KHODJA**[2] **and A BELASRI**[1]

[1] Laboratoire de Physique des Plasmas, Matériaux Conducteurs et leurs Applications, Université d'Oran des Sciences et de la Technologie USTO-MB, Faculté de Physique, Oran 31000, Algeria
[2] Unité de Recherche Appliquée en Energies Renouvelables, URAER, Centre de Développement des Energies Renouvelables, CDER, 47133, Ghardaïa, Algeria

E-mail: khadir.na.pl@gmail.com

Received 5 March 2017, revised 12 April 2017
Accepted for publication 13 April 2017
Published 26 July 2017

Abstract

In the present paper, we carried out a theoretical study of dielectric barrier discharge (DBD) filled with pure methane gas. The homogeneous discharge model used in this work includes a plasma chemistry unit, an electrical circuit, and the Boltzmann equation. The model was applied to the case of a sinusoidal voltage at a period frequency of 50 kHz and under a gas pressure of 600 Torr. We investigated the temporal variation of electrical and kinetic discharge parameters such as plasma and dielectric voltages, the discharge current density, electric field, deposited power density, and the species concentration. We also checked the physical model validity by comparing its results with experimental work. According to the results discussed herein, the dielectric capacitance is the parameter that has the greatest effect on the methane conversion and H_2/CH_4 ratio. This work enriches the knowledge for the improvement of DBD for CH_4 conversion and hydrogen production.

Keywords: methane plasma chemistry, dielectric barrier discharge, homogeneous discharge model, hydrogen production, methane conversion

(Some figures may appear in colour only in the online journal)

1. Introduction

According to many research works, hydrogen presents a promising future energy carrier that is free of carbon [1] and its principal attraction is that it has a wide diversity of production methods from a variety of resources. Hydrogen and other hydrocarbons can be produced by converting methane or carbon dioxide/methane mixtures by using plasma reforming [2–4], from biomass gasification [5–7], and from water by electrolysis [8] and it can be used to feed fuel cells and internal combustion engines to generate electrical and/or mechanical energy [9]. Dielectric barrier discharge (DBD) at atmospheric pressure possesses several applications such as ultraviolet generation [10], ozone production [11], and conversion of natural gas and hydrocarbons into synthesis gas (syngas). In our work, DBD is used to convert CH_4 into hydrogen and other hydrocarbon species. In the literature, we found several works that have studied the effect of many parameters on the conversion and hydrogen production. The discharge gap of DBD has a great effect on the CH_4 conversion. Wang *et al* [12] and Xu and Tu [2] studied experimentally a coaxial DBD reactor [12]; they reported that at discharge gaps of 0.4, 0.9, and 1.9 mm, the methane conversion has values of 25.10%, 20.01%, and 13.76%, respectively, and this means that the methane conversion is higher when the discharge gap is less than 1 mm. The methane conversion found by Xu and Tu [2] reached a maximum of 25.2% but at a feed flow and discharge power higher than those used by Wang *et al* [12]. Nguyen and Lee [13] proved that a pulse waveform enhanced the conversion of CO_2 and CH_4 and the selectivity to H_2 and CO compared with a sinusoidal waveform in a coaxial DBD reactor. Zhang *et al* [14] investigated experimentally a methane

conversion DBD reactor to find the most favorable parameters to obtain higher methane conversion and yields. This can be reached by using higher input power and smaller discharge distance. Ozkan *et al* [4] studied experimentally the effect of CO_2 and CH_4 flow rate, power, and carrier gas (Ar, He) on the conversion in a CO_2/CH_4 mixture with a multi-electrode DBD reactor and the results show that the conversion of CO_2 and CH_4 decreases with increasing gas flow rate and linearly increases with power. Concerning the carrier gas, CH_4 conversion is higher with He than with Ar and for CO_2 conversion they observed the opposite effect. Scapinello *et al* [15] showed that CH_4 and CO_2 conversions increase as a function of SEI (specific energy input) whereas H_2 selectivity is almost constant. Thanompongchart and Tippayawong [16] studied the effect of power input, flow rate, air addition, and number of reactors on CH_4 conversion and H_2 yield for the production of syngas by using a gliding arc plasma reactor fed with a CH_4/CO_2 mixture. They observe that high power input and lower flow rate enhance CH_4 conversion and H_2 yield and using two cascade reactors give higher conversions and yields than a single reactor. De Bie *et al* [17] developed a one-dimensional fluid model to convert CH_4 by using a DBD reactor into syngas, hydrocarbons, and oxygenated molecules and they conclude that a CH_4/CO_2 mixture favors the formation of H_2 more than the CH_4/O_2 mixture. Snoeckx *et al* [3] used a 0D chemical kinetics model developed by Kushner and co-workers [18, 19] to describe the plasma chemistry in a CH_4/CO_2 mixture and they calculated the density of the important species included in the plasma discharge (molecules, radicals, and ions) and the conversion and selectivities by variation of different parameters (discharge power, flow rates, and SEI). The continuation of this work [20] allowed the authors to study the influence of the operating parameters of the DBD reactor to determine which of them are the most promising in terms of energy efficiency and conversion. They obtained a conversion of 84% with an energy efficiency of 8.5% and they noted that increasing the CO_2 concentration in the mixture led to the increase of conversion and energy efficiency. Liu *et al* [21] performed a monoxidative conversion of CH_4 in a coaxial DBD reactor at atmospheric pressure aiming to produce H_2 and higher hydrocarbons. They developed a three-layer back-propagation artificial neutral network (ANN) model to investigate the system, which allowed them to obtain a CH_4 conversion of 36% at a discharge power of 75 W and with a selectivity of C_2H_6 of 42.4% and they also found that the discharge power is the most influential parameter. Levko and Tsymbalyuk [22] demonstrated that the concentration of molecular hydrogen is much higher in glow discharge (GD) compared with barrier discharge (BD) by using a model developed by Shchedrin *et al* [23]. Tu *et al* [24, 25] investigated a plasma-assisted catalytic dry reforming of CH_4/CO_2 by using a coaxial DBD reactor combined with and without a plasma-reduced Ni/Al_2O_3 catalyst to show the difference. They showed that the presence of the catalyst decreases the breakdown voltage and conversions of CH_4 and CO_2 but increases the H_2 selectivity. In [25], the addition of quartz wool improved the conversion of CH_4 in the plasma dry reforming reaction. In another work by Tu *et al* [26], an atmospheric pressure AC gliding arc reactor was developed for the plasma dry reforming of CH_4/CO_2. The use of this kind of plasma technology leads to improvements in the energy efficiency of dry reforming by the increase of the electron density in the gliding arc plasma. Jasiński *et al* [27–30] investigated atmospheric pressure microwave plasma to produce hydrogen by using CH_4 or a CH_4/gas mixture and they concluded that their plasma method for hydrogen generation is better than those used by others such as electron beam, gliding arc, plasmatron. Horng *et al* [31] used a small plasma converter to generate hydrogen and it was shown that under the optimal operating conditions, the plasma converter produced a maximum hydrogen concentration of 48%. In the work by Czylkowski *et al* [32], a combined steam reforming in microwave plasma technology for hydrogen production in CH_4/CO_2 was used for the first time. They obtained an energy yield of hydrogen production of 43 g(H_2) kWh^{-1}, which is not far from the US Department of Energy's energy yield requirement (60 g(H_2) kWh^{-1}). A direct conversion of CH_4/CO_2 by using dielectric barrier discharge plasma has been investigated by Zou *et al* [33, 34] to produce gaseous and liquid hydrocarbons, syngas, and oxygenates. They found that to achieve a large conversion of CH_4 and CO_2 and a high yield of hydrocarbons and acids, the discharge gap of 1.1 mm is preferred, whereas a 1.8 mm gap induces a more selective production of alcohols [33]. They introduced a starch coating on the dielectric, with a chemical formula of $(C_6H_{10}O_5)_n$ and they noted that this increased the selectivity of oxygenates significantly [34]. In [35], the authors gave comparative results for methane conversion in DBD and corona discharge. Their results showed that in DBD the main products are the saturated hydrocarbons (C_2H_6), and in corona discharge the unsaturated hydrocarbons (C_2H_2) are the dominant products. Other works can be found in the literature about plasma discharge in methane/gas mixtures. They are not related to hydrogen production applications but are applied for thin film deposition [36, 37]. The aim of this work is to optimize the methane conversion and H_2/CH_4 ratio, which is why it is important to better understand the plasma chemistry process. In this paper, we present the results of DBD reactor modeling filled with pure methane. These results concern the evolution of discharge current density, voltages, electric field, deposited power density, species density, methane conversion, and ratio with time. We also optimized the methane DBD reactor by investigating the effect of electrical parameters on some species density, methane conversion, and H_2/CH_4 ratio.

2. Model description

The model of homogeneous discharge used in this work is based on the Boltzmann equation and the plasma chemistry coupled to the electrical circuit. This model was developed to describe the electrical and kinetic characteristics of a pure CH_4 DBD reactor for hydrogen production. The dielectric layers are represented by two capacitances connected in series and C_d is their equivalent capacitance. The scheme of the methane DBD reactor is presented in figure 1.

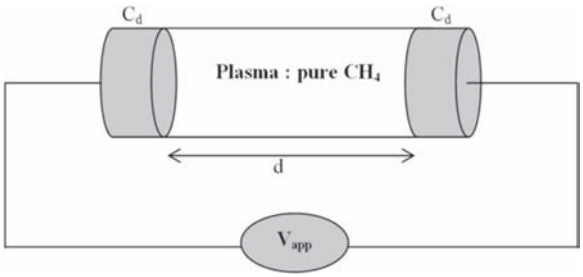

Figure 1. Discharge scheme.

The applied sinusoidal voltage through the discharge is given by the following formulae:

$$V_{app}(t) = V_p(t) + V_d(t) \quad (1)$$

where $V_p(t)$ and $V_d(t)$ represent the plasma and dielectric voltages across the discharge, respectively.

Species density is obtained by the resolution of the continuity equation:

$$\frac{d[X_i]}{dt} = S_i(t) \quad (2)$$

where $[X_i]$ is the concentration of species i at time t and $S_i(t)$ is the source term, which takes into account the species creation and loss under the collision effects.

The resolution of the equations system describing the dielectric and the plasma kinetic was done by using the classical GEAR method [38] between instants t and $t + dt$ for a given voltage at time t.

The kinetic scheme of pure CH_4 that we have developed is shown in table 1. It is made for seventeen different chemical species, which includes neutrals, radicals, ions, excited species, and electrons (see table 2).

The transport coefficients and the electronic collision frequencies, depending on the reduced electric field E/N, are tabulated by solving the steady-state homogeneous electron Boltzmann equation in pure methane, by using Bolsig+ solver [39].

The conversion of methane and H_2/CH_4 ratio are defined as:

$$\text{Conv}_{CH_4}(\%) = \frac{\text{mole of } CH_4 \text{ converted}}{\text{mole of } CH_4 \text{ input}} \times 100 \quad (3)$$

$$\text{Ratio}_{H_2/CH_4} = \frac{H_2 \text{ density produced}}{CH_4 \text{ density converted}} \times 100. \quad (4)$$

3. Results and discussion

We discuss in this section the results obtained from the homogeneous discharge model in the case of pure methane gas for different discharge parameters. These parameters and operating conditions are indicated in table 3.

3.1. Electrical discharge characteristics

In order to check the validity of the present model, we compared its results with experimental ones by using the same DBD reactor configuration as in Xu and Tu's work [2].

Figures 2(a) and (b) show the waveforms of applied voltage and current discharge during one and half periods, calculated with our numerical model and compared with those of [2]. From this comparison, one can see clearly that the model predicts correctly the waveform of the electrical characteristics of the discharge, which coincide with those measured in [2]. In particular, the value of the current peak calculated with the present model reaches a maximum value of 0. 34 A, which is on the order of that measured, 0.35 A.

Figure 3 shows the waveforms of applied voltage $V_{app}(t)$, dielectric voltage $V_d(t)$, and plasma voltage $V_p(t)$ for two periods at a peak value of applied voltage of 8 kV under total gas pressure of 600 Torr, gas temperature of 300 K, dielectric capacitance of 230 pF, and frequency of 50 kHz. The time for gas breakdown calculated corresponds to 0.35 μs. After the gas breakdown, the plasma voltage decreases in a very rapid manner, unlike the dielectric voltage, which increases.

In figure 4, the discharge current density is plotted. The peak reaches a value of 4.0 A cm^{-2} in the first half period. We can also observe that gas breakdown occurs at each half period.

The waveforms of the electric field and the deposed power density are plotted in figure 5. The magnitude of electric field and deposed power peaks (see figures 5(a) and (b), respectively) are constant after the first half cycle with values of 13.6 kV cm^{-1} and 49.11 kW cm^{-3}, respectively.

3.2. Methane plasma chemistry

The temporal profiles of species density at 8 kV under a pressure of 600 torr are depicted in figures 6(a) and (b). These figures show that after the breakdown phase, fast growth of excited, charged, neutral, and radical species densities are noticed. The reactions responsible for the species creation are listed in table 1 from R1 to R46.

3.2.1. Charged species density. The charged particles densities, which include electrons, CH_2^+, CH_3^+, CH_4^+, CH_5^+, and $C_2H_5^+$, are plotted in figure 6(a). Among the different hydrocarbon ions, the dominant ion in the plasma volume is $C_2H_5^+$ (R16, R18) with a peak density of 3.69 $\times$ 10^{12} cm^{-3} at 3.15 μs. The second dominant hydrocarbon ion is CH_5^+ (R14, R15) with a peak value of 1.28 $\times$ 10^{11} cm^{-3} at 3.05 μs. The CH_3^+ (R4, R19, R20, R21) and CH_4^+ (R2, R17, R23) peak densities reach values of 4.51 $\times$ 10^8 and 4.01 $\times$ 10^8 cm^{-3}, respectively, at the same time point. Moreover, both CH_3^+ and CH_4^+ are consumed to produce $C_2H_5^+$ and CH_5^+, respectively. This leads to a lowering of their density. Being four magnitude orders smaller than $C_2H_5^+$, the CH_2^+ (R7, R22) ion was found to be

Table 1. List of reaction processes and their rate coefficients used in our work (T_g is the gas temperature in Kelvin and rate coefficients are in $cm^3\ s^{-1}$).

	Reaction	Rate coefficient	References
Electron−molecule			
(R1)	$CH_4 + e \rightarrow CH_4^* + e$	(Tabulated)	[39]
(R2)	$CH_4 + e \rightarrow CH_4^+ + 2e$	(Tabulated)	[39]
(R3)	$CH_4 + e \rightarrow CH_2 + 2H + e$	(Tabulated)	[39]
(R4)	$CH_4 + e \rightarrow CH_3^+ + H + 2e$	$2.85 \times 10^{-12} T_g^{-0.835} \exp(-187172/T_g)$	[40]
(R5)	$CH_4 + e \rightarrow CH_3 + H + e$	$5.16 \times 10^{-5} T_g^{-0.642} \exp(-169882.6/T_g)$	[40]
(R6)	$CH_4 + e \rightarrow CH + H_2 + H + e$	$5.75 \times 10^{-4} T_g^{-0.828} \exp(-204462.5/T_g)$	[40]
(R7)	$CH_4 + e \rightarrow CH_2^+ + H_2 + 2e$	$6.29 \times 10^{-14} T_g^{-0.532} \exp(-204758.2/T_g)$	[40]
(R8)	$C_2H_6 + e \rightarrow C_2H_5 + H + e$	$1.53 \times 10^{-7} T_g^{-0.06} \exp(-121377.8/T_g)$	[40]
(R9)	$C_2H_6 + e \rightarrow C_2H_4 + H_2 + e$	$1.35 \times 10^{-6} T_g^{-0.135} \exp(-226394.1/T_g)$	[40]
Electron–ion recombination			
(R10)	$CH_4^+ + e \rightarrow CH_3 + H$	$1.7 \times 10^{-7} (300/T_g)^{0.5}$	[41]
(R11)	$CH_4^+ + e \rightarrow CH_2 + 2H$	$1.7 \times 10^{-7} \times (300/T_g)^{0.5}$	[41]
(R12)	$CH_3^+ + e \rightarrow CH_2 + H$	$3.5 \times 10^{-7} \times (300/T_g)^{0.5}$	[41]
(R13)	$C_2H_5^+ + e \rightarrow C_2H_3 + 2H$	$7.4 \times 10^{-7} \times (300/T_g)^{0.5}$	[41]
Ion–molecule			
(R14)	$CH_4^+ + CH_4 \rightarrow CH_5^+ + CH_3$	1.5×10^{-9}	[42]
(R15)	$CH_4^+ + H_2 \rightarrow CH_5^+ + H$	3.30×10^{-11}	[43]
(R16)	$CH_3^+ + CH_4 \rightarrow C_2H_5^+ + H_2$	1.20×10^{-9}	[42]
(R17)	$CH_3^+ + CH_4 \rightarrow CH_4^+ + CH_3$	$1.\ 36 \times 10^{-10}$	[44]
(R18)	$CH_2^+ + CH_4 \rightarrow C_2H_5^+ + H$	3×10^{-10}	[43]
(R19)	$CH_2^+ + H_2 \rightarrow CH_3^+ + H$	1.6×10^{-9}	[43]
(R20)	$CH_5^+ + CH_2 \rightarrow CH_3^+ + CH_4$	9.60×10^{-10}	[43]
Ion−atom			
(R21)	$CH_4^+ + H \rightarrow CH_3^+ + H_2$	1.10×10^{-11}	[41]
(R22)	$CH_3^+ + H \rightarrow CH_2^+ + H_2$	7.00×10^{-10}	[43]
(R23)	$CH_5^+ + H \rightarrow CH_4^+ + H_2$	1.5×10^{-10}	[43]
Molecule−atom			
(R24)	$CH_4 + H \rightarrow CH_3 + H_2$	5.80×10^{-13}	[43]
(R25)	$CH_3 + H \rightarrow CH_2 + H_2$	$1.00 \times 10^{-10} \exp(-7600/T_g)$	[44]
(R26)	$CH_2 + H \rightarrow CH + H_2$	7.7×10^{-10}	[43]
(R27)	$C_2H_6 + H \rightarrow C_2H_5 + H_2$	$2.4 \times 10^{-13} \exp(-3730/T_g)$	[44]
(R28)	$C_2H_5 + H \rightarrow C_2H_4 + H_2$	3.00×10^{-12}	[43]
(R29)	$C_2H_4 + H \rightarrow C_2H_3 + H_2$	$9.00 \times 10^{-10} \exp(-7500/T_g)$	[44]
(R30)	$C_2H_5 + H \rightarrow C_2H_6$	6.00×10^{-11}	[43]
(R31)	$C_2H_5 + H \rightarrow 2CH_3$	6.00×10^{-11}	[43]
Molecule−molecule			
(R32)	$CH_4 + CH_3 \rightarrow C_2H_5 + H_2$	1.70×10^{-11}	[43]
(R33)	$CH_4 + CH_2 \rightarrow C_2H_4 + H_2$	1.70×10^{-11}	[43]
(R34)	$CH_3 + CH_3 \rightarrow C_2H_4 + H_2$	$1.70 \times 10^{-8} \exp(-16000/T_g)$	[44]
(R35)	$CH_2 + CH_2 \rightarrow C_2H_2 + H_2$	$2.00 \times 10^{-11} \exp(-400/T_g)$	[44]
(R36)	$CH_3 + CH_3 \rightarrow C_2H_5 + H$	$5.00 \times 10^{-11} \exp(-6800/T_g)$	[44]
(R37)	$CH_2 + CH \rightarrow C_2H_2 + H$	2.00×10^{-11}	[43]
(R38)	$CH + H_2 \rightarrow CH_2 + H$	$3.75 \times 10^{-10} \exp(-1660/T_g)$	[43]
(R39)	$CH_4 + CH \rightarrow C_2H_5$	1.00×10^{-10}	[43]
(R40)	$CH_4 + CH_2 \rightarrow CH_3 + CH_3$	7.00×10^{-12}	[43]
(R41)	$CH_3 + CH_3 \rightarrow C_2H_6$	$8.00 \times 10^{-11}/6.00 \times 10^{-11}$	[42]
(R42)	$CH_2 + CH_2 \rightarrow C_2H_4$	1.70×10^{-12}	[44]
(R43)	$CH + CH_4 \rightarrow C_2H_5$	1.00×10^{-10}	[43]
(R44)	$CH + CH \rightarrow C_2H_2$	2.00×10^{-10}	[44]
(R45)	$C_2H_5 + C_2H_5 \rightarrow C_2H_6 + C_2H_4$	2.00×10^{-12}	[43]
(R46)	$C_2H_6 + CH_2 \rightarrow C_3H_8$	4.00×10^{-10}	[43]

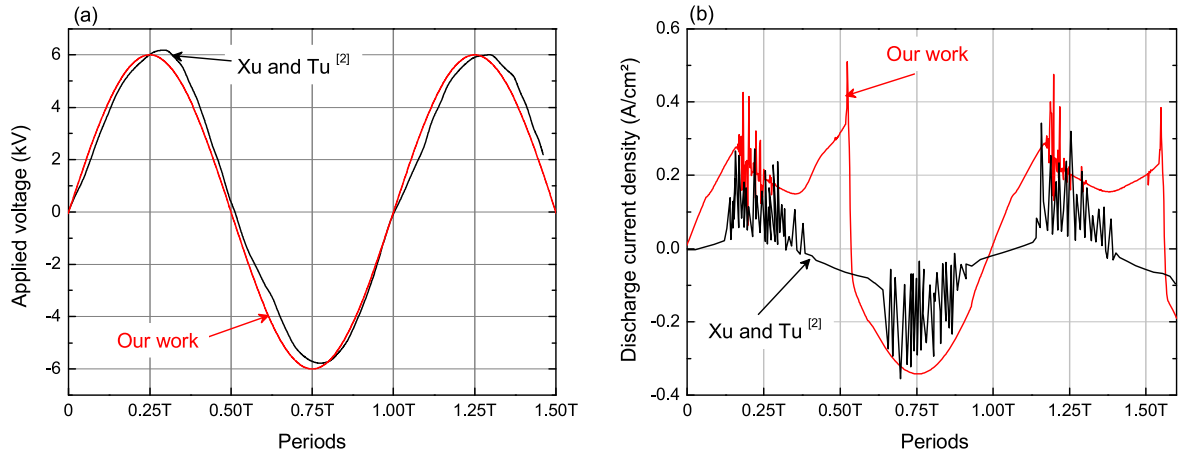

Figure 2. Waveform comparison of (a) applied voltage and (b) discharge current density.

Table 2. Different species taken into account in our model.

Neutrals	Ions	Radicals	Electrons and excited species
CH_4	CH_4^+	C_2H_5	e^-
C_2H_6	CH_2^+	CH	CH_4^*
C_2H_4	CH_3^+	CH_2	
C_2H_2	$C_2H_5^+$	CH_3	
H_2	CH_5^+	H	

Table 3. Methane DBD reactor parameters and operating conditions.

Parameter	Value
Gas	Methane (CH_4)
Gas pressure	$p = 380$–1520 Torr
Gap length	$d = 0.4$ cm
Gas temperature	$T_g = 250$–400 K
Electrode area	$A = 1$ cm^2
Dielectric capacitance	$C_d = 1$–1000 pF
Initial electron density	$ne_0 = 10^9$ cm^{-3}
Peak value of applied voltage	$V_s = 6$–12 kV
Sinusoidal waveform	$V_{app}(t) = V_s \sin(2\pi ft)$
Frequency	$f = 50$ kHz–1 MHz

the least dominant due to its consumption by $C_2H_5^+$ and CH_3^+ to create hydrogen atoms.

3.2.2. H_2 production. In order to investigate the production of molecular hydrogen, we plotted in figure 6(b) the temporal profiles of species density. Many chemical reactions increase hydrogen production though hydrocarbon species dissociation. The reactions responsible for H_2 formation are given by R7 and R9, which present electron impact dissociation of CH_4 and C_2H_6, R16 is the molecule−ion reaction, R21−R23 are ion −atom reactions, R24−R29 are molecule−atom reactions, and R32−R35 are molecular reactions. H_2 density reaches its highest value of 2.43×10^{18} cm^{-3} at the end of discharge.

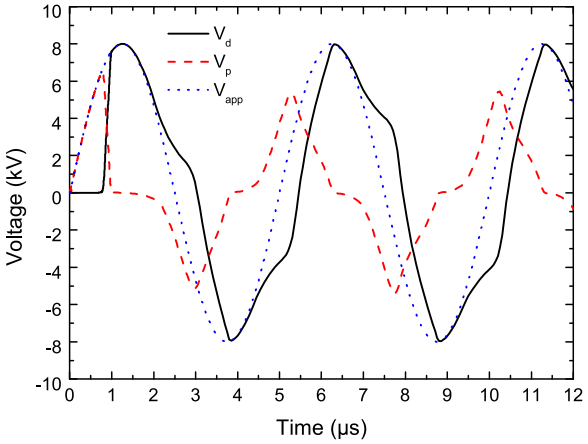

Figure 3. Waveforms of V_d: dielectric, V_p: plasma, V_{app}: applied voltage.

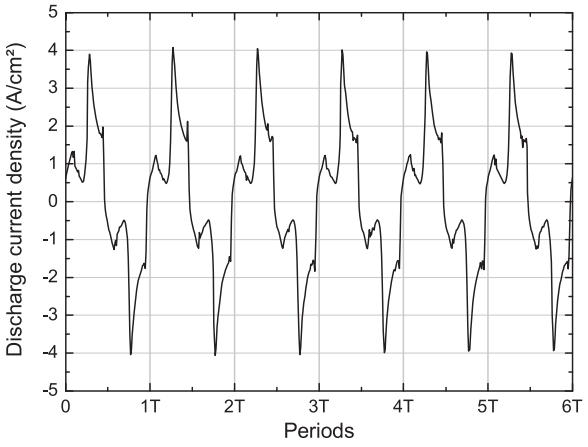

Figure 4. Waveforms of discharge current density for six periods.

3.2.3. Production of other species. The time variation of CH_4^*, neutral, and radical species during the plasma discharge is shown in figure 6(b). Atomic hydrogen was

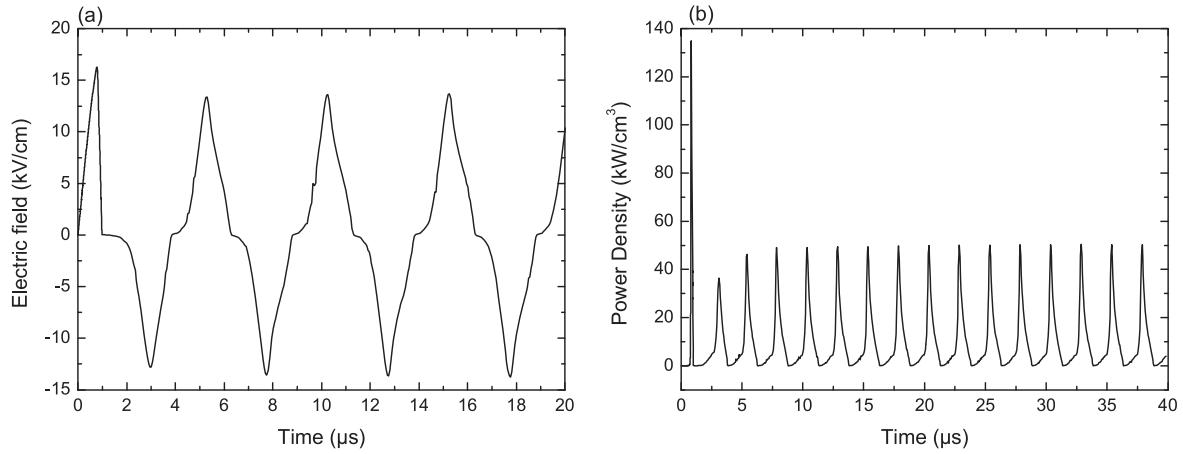

Figure 5. Time evolution of (a) the electric field and (b) deposed power density.

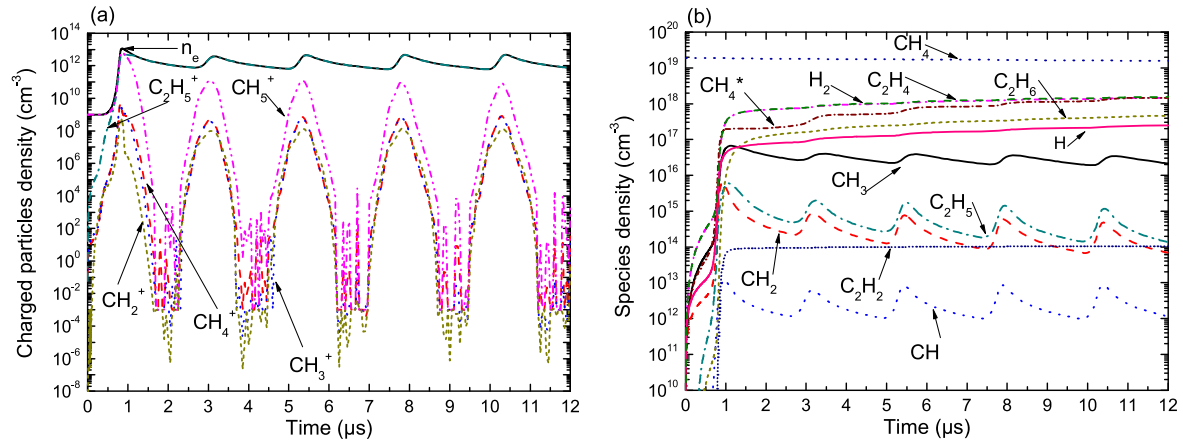

Figure 6. Time evolution of the concentration of (a) charged particles and (b) molecules and excited particles.

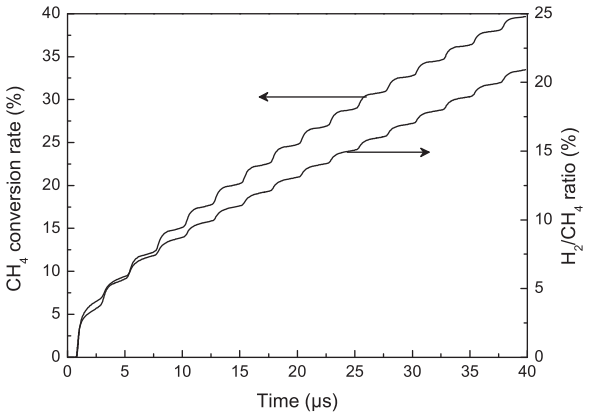

Figure 7. Time evolution of CH_4 conversion and H_2/CH_4 ratio.

found to be the dominant radical. The highest density of H observed in the plasma volume is $6.06 \times 10^{17}\,\mathrm{cm}^{-3}$. It is created from CH_4 and C_2H_6 dissociation, CH_2, CH_3, C_2H_2, and C_2H_5 recombination and from ion−molecule reactions (see reactions R15, R18, and R19).

The recombination of two CH_3 radicals leads to ethane production (C_2H_6) according to reaction R41. Ethane density reaches a value of $1.01 \times 10^{18}\,\mathrm{cm}^{-3}$. R30 and R45 also lead to the production of ethane but are less probable. Indeed, as we can see in figure 6(b), C_2H_5 density is lower by one order of magnitude than that of CH_3. CH_4^* reaches its maximum value of $4.42 \times 10^{18}\,\mathrm{cm}^{-3}$ at the end of discharge.

3.3. Methane conversion by non-thermal plasma

3.3.1. Conversion and H_2/CH_4 ratio. Figure 7 shows the methane conversion and the H_2/CH_4 ratio as a function of time. They increased rapidly to 39.67% and 20.91%, respectively, during the discharge. This is due to methane dissociation by electron collision, atom−molecule, ion −molecule, and molecule−molecule reactions, which synthesized different hydrocarbon species.

3.3.2. Conversion and deposited energy for different periods. In figure 8, we present the evolution of the CH_4 conversion and energy for ten periods. They vary from 9.1% to 60.46% and from 5.63 J to 274.61 J, respectively.

3.3.3. Input voltage effect. One can see from figure 9 that the current density increases with the increase of applied voltage. The peak values of the current density are 3.11, 3.9, and

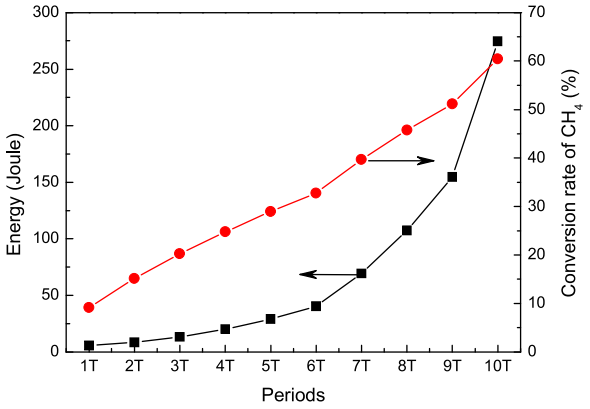

Figure 8. Variation of CH_4 conversion and energy for ten periods.

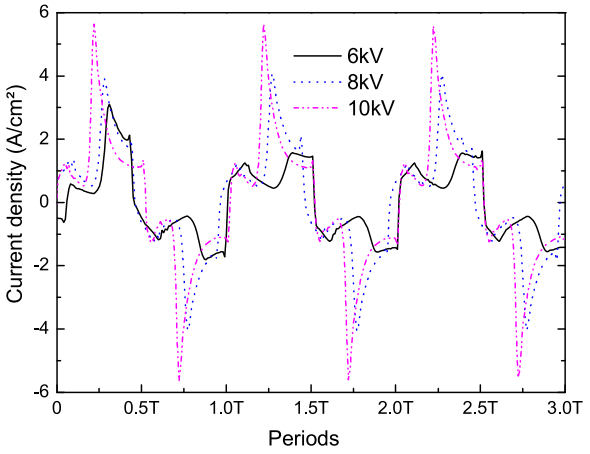

Figure 9. Time evolution of discharge current density for different values of applied voltages.

5.63 A cm^{-2} at 6, 8, and 10 kV, respectively. However, the breakdown time increases when the applied voltage decreases.

The conversion of CH_4 and H_2/CH_4 ratio almost linearly increase with increasing applied voltage as shown in figure 10(a). The CH_4 conversion and H_2/CH_4 ratio increase to 36.07% and 16.85%, respectively, at an applied voltage of 12 kV. The electron and C_2H_5 densities are the most affected by the applied voltage. They increase to 6.99 $\times$ 10^{11} cm^{-3} and 7.13 $\times$ 10^{14} cm^{-3}, respectively, at 12 kV (see figure 10(b)).

3.3.4. Dielectric capacitance effect. The effect of the dielectric capacitance on the methane conversion, H_2/CH_4 ratio, and species density is shown in figure 11. The increase in capacitance has a great effect on the conversion and the ratio. Indeed, they evolve from 2.66% at 1 pF to 58.03% and from 2.48% at 1 pF to 28.75%, respectively (see figure 11(a)). Concerning the species density plotted in figure 11(b), the more affected particles are the electrons, ethylene, ethane, and hydrogen. They increase almost by one or two magnitude and reach their high values of 9.56 $\times$ 10^{11}, 1.93 $\times$ 10^{18}, 1.14 $\times$ 10^{18}, and 2.32 $\times$ 10^{18} cm^{-3}, respectively at 1 nF.

3.3.5. Gas pressure effect. As can be seen in figure 12(a), the pressure has a significant effect on the conversion and ratio. Indeed, both of them decrease, from 32.41% to 17.06% and from 14.96% to 12.12%, respectively, with increasing gas pressure.

The increasing gas pressure has only a slight effect on CH_3 density, but for the rest of species it has a significant impact on their density. The electron and C_2H_5 density decrease to 7.4 $\times$ 10^{11} and 2.21 $\times$ 10^{14} cm^{-3}, respectively. C_2H_4, C_2H_6, and H_2 increase to 4.77 $\times$ 10^{18}, 1.17 $\times$ 10^{18}, and 4.92 $\times$ 10^{18} cm^{-3}, respectively. This is shown in figure 12(b).

Our calculations allowed us to demonstrate that the electron density, conversion and H_2/CH_4 ratio decrease with decreasing gas pressure. This is because at high pressure the mean free path of electrons becomes smaller and electrons lose their energy much faster, leading to the reduction of electron density [36]. According to the electron reactions taken into account in this work (see table 1), most of them represent collisions with CH_4, which is why the conversion and H_2/CH_4 ratio are affected by the decreasing electron density.

3.3.6. Gas temperature effect. Figure 13(a) shows the CH_4 conversion and H_2/CH_4 ratio versus gas temperature in the range between 250 K and 400 K. The CH_4 conversion decreases by 0.5%, whereas the H_2/CH_4 ratio increases by 0.39% with the gas temperature rising. We noted that the gas temperature thus has almost no effect on conversion and ratio. In figure 13(b), the H_2 density increases from 1.88 $\times$ 10^{18} cm^{-3} to 1.94 $\times$ 10^{18} cm^{-3}, so we can say that there is only a slight increase and this is noted for each value of species density.

3.3.7. Frequency effect. The methane conversion increases from 23.86% at 50 kHz to 24.78% at 200 kHz; after this last frequency, it begins to decrease until reaching 22.7% at 1 MHz, whereas the H_2/CH_4 ratio decreases from 14.86% to 10.42% on increasing frequency (see figure 14(a)).

The variation of the frequency from 50 kHz to 1 MHz has an increasing effect on the electron, CH_3, and C_2H_5 densities. They reach maximum values of 3.16 $\times$ 10^{12} cm^{-3}, 4.69 $\times$ 10^{16} cm^{-3}, and 4.34 $\times$ 10^{14} cm^{-3}, respectively. But for the C_2H_4, C_2H_6, and H_2 densities (see figure 14(b)), the frequency has a slight decreasing effect. They reach minimum values of 1.42 $\times$ 10^{18} cm^{-3}, 5.20 $\times$ 10^{17} cm^{-3}, and 1.55 $\times$ 10^{18} cm^{-3}, respectively.

4. Conclusion

The methane DBD reactor at atmospheric pressure was studied by developing a homogeneous discharge model, which was applied under the operating conditions cited in table 3 for hydrogen production. This model includes a plasma

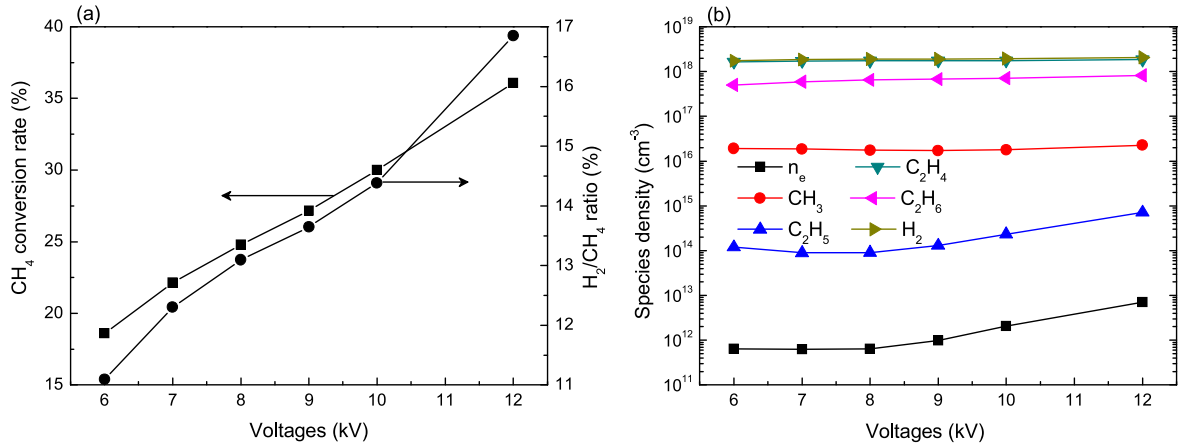

Figure 10. Effect of applied voltages on (a) CH_4 conversion and H_2/CH_4 ratio and (b) species density.

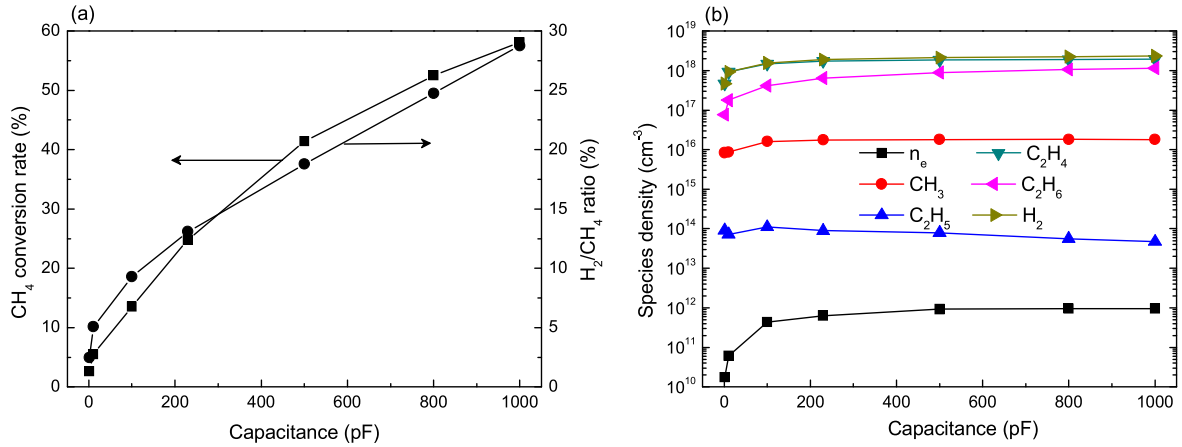

Figure 11. Effect of dielectric capacitance on (a) CH_4 conversion and H_2/CH_4 ratio and (b) species density.

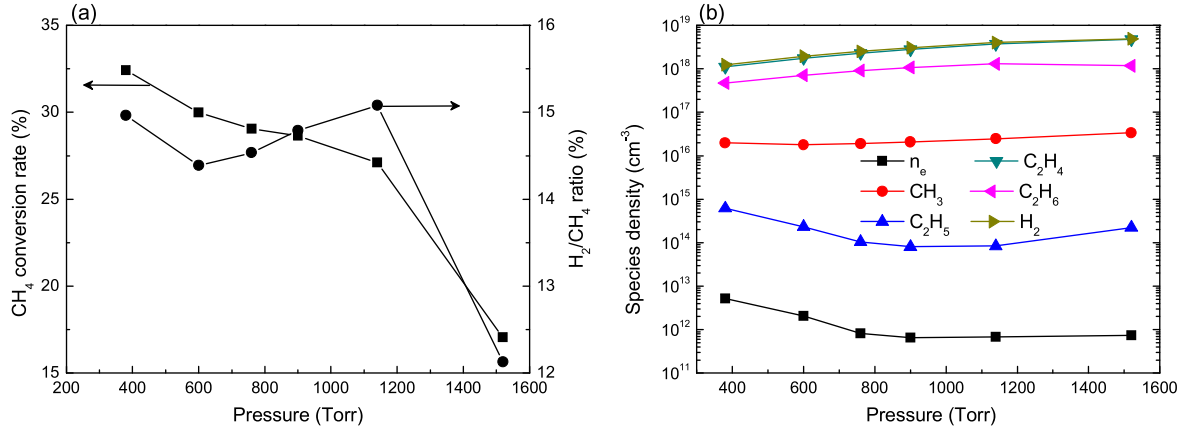

Figure 12. Effect of gas pressure on (a) CH_4 conversion and H_2/CH_4 ratio and (b) species density.

chemistry module, a circuit module and the Boltzmann equation module to investigate the electrical and physical characteristics of high-pressure DBD.

In the beginning of this paper, the validity of the physical model was checked by comparison with experimental work, and then the model was applied in the case of a sinusoidal voltage at period frequencies in the range 50 kHz–1 MHz.

The results discuss the discharge characteristics and the optimization of the H_2 production. We calculated the neutral, ion, radical, electrons and excited species densities. The methane conversion and H_2/CH_4 ratio were also calculated and reached 39.67% and 20.91%, respectively, during the discharge. Finally, the parametrical study allowed us to say that the dielectric capacitance and the applied voltage have a significant impact on the methane conversion and H_2/CH_4

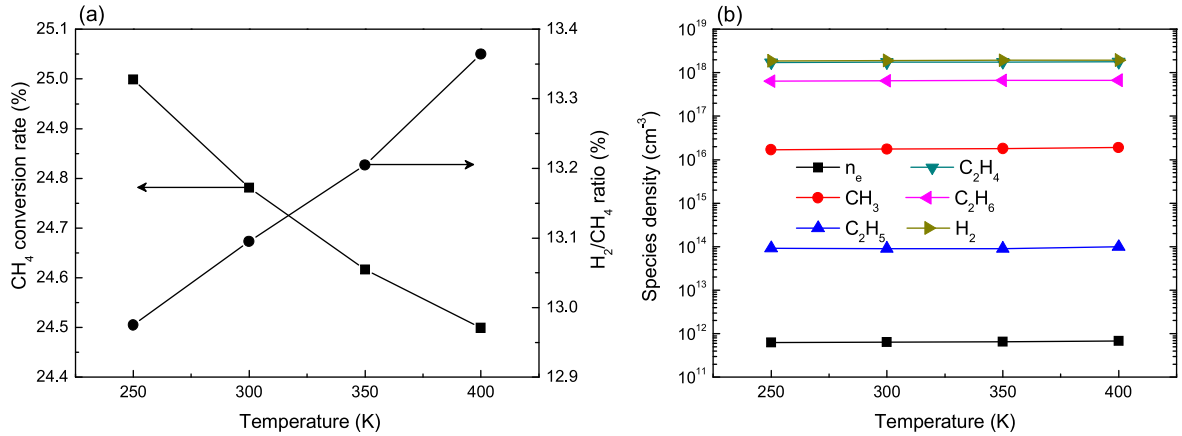

Figure 13. Effect of gas temperature on (a) CH_4 conversion and H_2/CH_4 ratio and (b) species density.

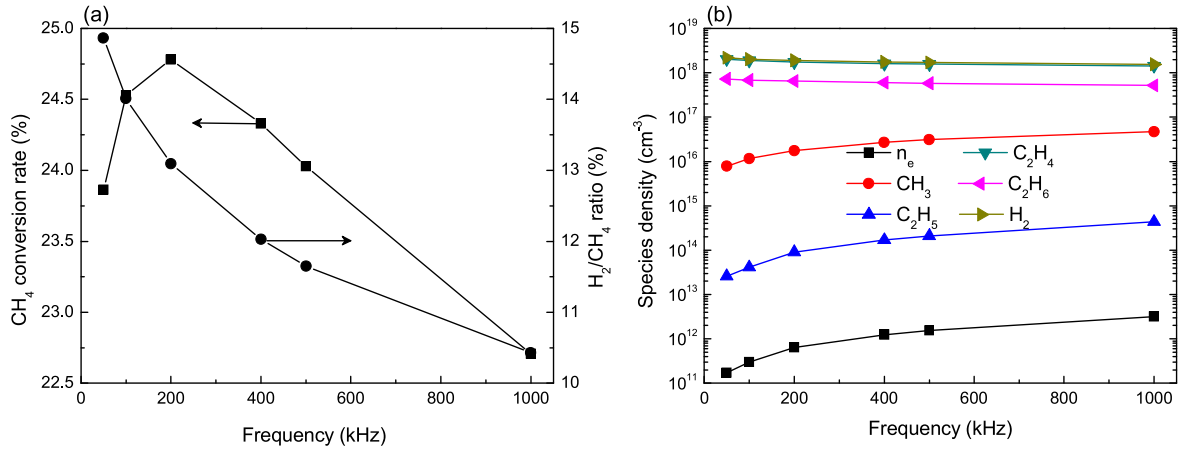

Figure 14. Effect of frequency on (a) CH_4 conversion and H_2/CH_4 ratio and (b) species density.

ratio. They reached values of 58.03% and 28.75%, respectively. Also, our results suggest that to maximize the H_2 density production for a given sinusoidal applied voltage, high gas pressure and high dielectric capacitance are required.

References

[1] Züttel A, Borgschulte A and Schlapbach L 2007 *Hydrogen as a Future Energy Carrier* (Weinheim: Wiley)
[2] Xu C and Tu X 2013 *J. Energy Chem.* **22** 420
[3] Snoeckx R *et al* 2013 *J. Phys. Chem.* C **117** 4957
[4] Ozkan A *et al* 2015 *J. CO_2 Util.* **9** 74
[5] Rumpel S *et al* 2014 *Energy Environ. Sci.* **7** 3296
[6] Kruse O and Hankamer B 2010 *Curr. Opin. Biotechnol.* **21** 238
[7] Hwang J-H *et al* 2014 *Energy* **78** 887
[8] Zeng K and Zhang D K 2010 *Prog. Energ. Combust. Sci.* **36** 307
[9] Minić D 2012 *Hydrogen Energy: Challenges and Perspectives* (Croatia: InTeOp)
[10] Kogelschatz U 2012 *J. Opt. Technol.* **79** 484
[11] Benyamina M, Belasri A and Khodja K 2014 *Ozone: Sci. Eng.* **36** 253
[12] Wang B W *et al* 2013 *J. Energy Chem.* **22** 876
[13] Nguyen D B and Lee W G 2015 *Korean J. Chem. Eng.* **32** 62
[14] Zhang X *et al* 2009 *Chin. J. Chem. Eng.* **17** 625
[15] Scapinello M *et al* 2016 *J. Phys. D: Appl. Phys.* **49** 075602
[16] Thanompongchart P and Tippayawong N 2014 *Int. J. Chem. Eng.* **2014** 609836
[17] De Bie C *et al* 2011 *Plasma Process. Polym.* **8** 1033
[18] Dorai R, Hassouni K and Kushner M J 2000 *J. Appl. Phys.* **88** 6060
[19] Dorai R 2002 Modeling of atmospheric pressure plasma processing of gases and surfaces *PhD Dissertation* University of Illinois, Champaign, IL
[20] Snoeckx R *et al* 2015 *RSC Adv.* **5** 29799
[21] Liu S Y *et al* 2014 *J. Phys. Chem.* C **118** 10686
[22] Levko D S and Tsymbalyuk A N 2015 *Tech. Phys Lett.* **41** 228
[23] Shchedrin A I *et al* 2008 *JETP Lett.* **88** 99
[24] Tu X *et al* 2011 *J. Phys. D: Appl. Phys.* **44** 274007
[25] Tu X and Whitehead J C 2012 *Appl. Catal. B: Environ.* **125** 439
[26] Tu X and Whitehead J C 2014 *Int. J. Hydrogen Energy* **39** 9658
[27] Jasiński M, Dors M and Mizeraczyk J 2008 *J. Power Sources* **181** 41
[28] Jasiński M, Dors M and Mizeraczyk J 2009 *Eur. Phys. J.* D **54** 179
[29] Jasiński M *et al* 2011 *J. Phys. D: Appl. Phys.* **44** 194002
[30] Jasiński M *et al* 2013 *Int. J. Hydrogen Energy* **38** 11473
[31] Horng R-F *et al* 2007 *Fuel* **86** 81
[32] Czylkowski D *et al* 2016 *Energy* **113** 653
[33] Zou J J *et al* 2002 *Acta Phys. -Chim. Sin.* **18** 759
[34] Zou J J *et al* 2003 *Plasma Chem. Plasma Process.* **23** 69
[35] Zou J and Liu C-J 2004 *Plasma Sci. Technol.* **6** 2585

[36] Farouk T *et al* 2008 *J. Phys. D: Appl. Phys.* **41** 175202
[37] Oda A, Suda Y and Okita A 2008 *Thin Solid Films* **516** 6570
[38] Gear C W 1971 *Numerical Initial Value Problems in Ordinary Differential Equations* (Englewood Cliffs, NJ: Prentice-Hall)
[39] BOLSIG+: Electron Boltzmann equation solver (http://bolsig.laplace.univ-tlse.fr/)
[40] Yang Y 2003 *Plasma Chem. Plasma Process.* **23** 327
[41] Kosarev I N *et al* 2009 *Combust. Flame* **156** 221
[42] Herrebout D *et al* 2001 *J. Appl. Phys.* **90** 570
[43] Mao M and Bogaerts A 2010 *J. Phys. D: Appl. Phys.* **43** 205201
[44] Denysenko I B *et al* 2004 *J. Appl. Phys.* **95** 2713